IEEE Access
Multidisciplinary | Rapid Review | Open Access Journal

Received 11 April 2023, accepted 7 May 2023, date of publication 10 May 2023, date of current version 16 May 2023.

Digital Object Identifier 10.1109/ACCESS.2023.3275016

RESEARCH ARTICLE

A Unified Model for Multi-Satellite Imaging Mission Planning in Various Scenarios

XUEYING YANG, MIN HU, RUI ZHANG, AND GANG HUANG
Department of Aerospace Science and Technology, Space Engineering University, Beijing 101416, China

Corresponding author: Min Hu (jlhm09@126.com)

This work was supported by the National Natural Science Foundation of China under Grant 61403416.

ABSTRACT Multi-satellite imaging mission planning (MSIMP) has been difficult in various scenarios due to the complex constraints of multi-satellite imaging, the wide area covered by target points, and the difficulty of achieving different mission requirements in a short period of time with limited satellite resources. In addressing this challenge, this work investigates multi-satellite imaging mission planning based on the Unified Plan Model and Improved Adaptive Differential Evolution algorithm (UPM-IADE). First, a unified model is built based on two scenarios: a large-scale imaging mission and an emergency support mission, and then a mission assignment framework is adaptively selected based on mission priority. Second, a monorail task synthesis method based on visible time windows is created to clarify the execution relationship between the satellite and the target point. Finally, an individual weight ranking rule is developed, and the weight is used to combine the fitness value ranking and diversity ranking into a final fitness value ranking, which is used to select individuals that satisfy the mutation requirements into the mutation strategy pool for adaptive mutation strategy selection. Experiments 1, 2, 3, and 4 have demonstrated that UPM-IADE can successfully resolve the imaging satellite mission planning for both scenarios while providing remarkable performance in terms of high mission benefit and rapid response.

INDEX TERMS Multi-satellite imaging mission planning, global large-scale imaging mission, emergency support mission, adaptive differential evolution algorithm, individual weight ranking rule.

I. INTRODUCTION

Multi-Satellite Imaging Mission Planning (MSIMP) is the rational and optimal allocation of limited satellite resources based on numerous planning environments and types of observation requirements in order to improve the operational efficiency of Earth observation for gathering remote sensing images [1], [2]. With the ongoing development of satellite Earth observation applications and the gradual increase in the number and types of Earth observation satellites in orbit, user needs are becoming increasingly complicated. Maneuverability and orbital constraints prevent single-imaging satellites from providing continuous observations of individual target points [3], [4]. Owing to a large number of distributed satellites and the wide distribution area, multi-satellite missions can achieve long-term, multi-directional continuous monitoring of the observation area, which is widely used in disaster monitoring, urban planning, agriculture, meteorology, environmental protection, and many other fields. MSIMP is currently used extensively in practical applications such as large-scale imaging missions and emergency support missions. However, the difficulty of achieving different mission requirements in a short period of time with limited satellite resources. Therefore, it is important to study the problem of a unified model for MSIMP in various scenarios [5], [6].

In recent years, researchers have proposed numerous excellent models and algorithms that have demonstrated good performance in dealing with MSIMP.

Integer planning model based on satellite mission planning. The Integer Programming Model (IPM) is used in MSIMP to describe linearly constrained problems that can be solved using column generation methods to find the optimal solution [7]. Niu et al. [8] proposed a multi-objective integer planning model to efficiently allocate multiple satellites for

The associate editor coordinating the review of this manuscript and approving it for publication was Xiwang Dong.

large-area seismic image data acquisition and to solve the large-scale MSIMP target scheduling problem. Chen et al. [9] investigated the conflicting metrics for all visible time windows in the emergency mission and proposed a mixed integer linear programming model that satisfied the time interval constraint in order to solve the problem of limited observational capability in MSIMP.

Constraint satisfaction model based on satellite mission planning. The Constraint Satisfaction Problem (CSP) describes the non-linear goal and constraints in the MSIMP problem by combining the constraint satisfaction problem and the optimization objective so that the objective function is chosen as the minimum [10]. Wu et al. [11] proposed an improved constraint fulfillment model for NSGA-III MSIMP based on the imaging scheduling problem for large-scale satellite formation systems. Chen et al. [12] studied a constraint satisfaction model-based MSIMP for data subject scheduling, which solves the challenge of scheduling large-scale satellite observation data using an enhanced non-dominated ranking genetic algorithm. Zhang et al. [13] proposed a large-scale multi-satellite mission planning algorithm based on SVM+NSGA-II, which considers the periodicity of satellite resource conflict, the large-scale characteristics of multi-star missions, and the optimization objective constraint satisfaction model.

Deterministic Algorithm based on satellite mission planning. The Deterministic Algorithm (DA) is a local optimization algorithm based on a deterministic strategy that is more efficient for solving MSIMP problems with low problem complexity and small observation task size and less efficient for solving complex, larger-scale MSIMP problems [14]. Wang et al. [15] proposed an emergency MSIMP algorithm that takes into account cloud uncertainty using an integer linear model and branch delimitation combined with columns. She et al. [16] regarded the planning process as a dynamic combinatorial optimization problem with the highest priority and the smallest swing angle. To improve satellite observation efficiency, an MSIMP based on improved mixed integer programming is proposed.

Heuristic Algorithm based on satellite mission planning. The Heuristic Algorithm (HA) is an experience-based combinatorial optimization algorithm that can solve large-scale MSIMP problems effectively. However, this algorithm's application scope is limited, and reasonable heuristic rules must be constructed to obtain heuristic information [17]. Chen et al. [18] proposed a heuristic local search algorithm-based integrated scheduling method for Earth observation satellites to solve the large-scale MSIMP problem, and their local search algorithm ensures the algorithm's optimal performance. He et al. [19] used an edge computing framework and a heuristic planning algorithm to plan missions for multiple agile satellites, achieving a high mission completion rate by scheduling each satellite mission reasonably based on scheduling cycle order. Song et al. [20] proposed a heuristic algorithm for task selection time windows and adopted a multi-objective optimization algorithm to solve the multi-satellite mission planning problem.

Intelligent Optimization Algorithm based on satellite mission planning. The Intelligent Optimization Algorithm (IOA) is a well-established global optimization algorithm that is not limited to specific problems and is suitable for large-scale solution problems [21]. Zheng et al. [22] investigated an improved genetic algorithm based on a realistic space mission environment, which improved the mutation and crossover operators to significantly improve the efficiency and accuracy of swarm satellites performing complex tasks. Luo et al. [23] used an adaptive DE algorithm to investigate orbital maneuver optimization of earth observation satellites. Their research sheds new light on how to optimize the emergency mission-oriented earth satellite observation orbit maneuvering problem in three dimensions: optimal response time, ground resolution, and fuel consumption. Sun et al. [24] established an emergency task planning model and proposed a multi-strategy differential evolution algorithm based on the time window segmentation method to solve the problem.

Although the previous research produced good mission planning results, there are still the following challenges in multi-satellite mission planning when both large-scale imaging missions and emergency support missions are considered in two special scenarios:

- In the process of MSIMP, faced with the requirement of multi-satellite mission planning in various scenarios, research on MSIMP in only a single scenario faces the difficulties of inconsistent planning model and extended planning time. Therefore, how to construct a unified model for MSIMP in various scenarios is one of the challenges of MSIMP problem-solving.
- In practice, MSIMP is constrained by resources such as poor satellite maneuvering performance and the limited number of imaging times, as well as complex constraints of multi-imaging satellites in the mission environment, existing difficult problems such as low execution efficiency, multiple execution schemes, and long planning time. Therefore, how to construct a fast and accurate algorithm to solve the MSIMP scheme is another challenge for MSIMP problem-solving.

To address these difficulties, by using imaging satellites as the research object, large-scale imaging missions and emergency assurance missions as the planning scenarios, short planning times and high planning efficiency as the research objectives, this work investigates MSIMP based on the Unified Plan Model and Improved Adaptive Differential Evolution algorithm (UPM-IADE). The main contributions of this paper are outlined as follows:

- In terms of constructing planning models, for the challenge of the model inconsistency of multi-satellite mission planning in various scenarios. We build a unified model for the first time based on optimization theory for two scenarios: a large-scale imaging mission and an emergency support mission. We then adaptively choose

a mission assignment framework based on the priority of the mission, resolving issues with poor model scalability and weak algorithm targeting in the mission assignment of MSIMP for various users' actual needs.

- In terms of constructing mission planning algorithms, to address the poor side-swing maneuverability of the imaging satellites and the limited number of side-view images within each orbital revolution, we propose a single-orbit task synthesis method considering the time window. By adjusting the side view of the imaging satellite to combine several point targets into the observation strip at the same time to carry out the observation target task, in order to improve the execution efficiency of MSIMP.
- In terms of constructing adaptive algorithms, for the above two different scenarios, which have difficulties such as multiple execution options and long planning time, we investigate MSIMP based on the UPM-IADE algorithm. By considering individual fitness value and diversity contribution, an individual weight ranking rule and an adaptive mutation strategy pool are established. This method ensures that the optimal MSIMP execution scheme is obtained in a short time.

The remainder of the paper is organized as follows. Section II describes common approaches and classical differential evolutionary algorithms for two scenarios: multi-satellite mission-based planning for large-scale imaging missions and emergency support missions. Section III introduces the MSIMP unified model based on task priority, including a mathematical description of the model, the objective function, constraints, and evaluation indicators. Section IV presents the monorail task synthesis method based on visible time windows, as well as the principle and specific process of the UPM-IADE algorithm. Section V sets up simulation experiments and compares the performance of different algorithms. Section VI concludes and future perspectives.

II. RELATED WORD

This section first introduces the basic process of MSIMP and then introduces the basic concepts and principles of the differential evolution algorithm.

A. BASIC PROCESS OF MSIMP

MSIMP is aim to allocate satellite resources based on optimization theory for multiple imaging satellites and a large number of observation mission requirements proposed by users while taking into account multiple conflicting objective constraints, in order to clarify the specific information of observation missions and the corresponding executing satellites, orbit cycles, imaging time range, and the side view, and to maximize the overall benefit [25], [26], [27].

Assume that a set of observation tasks $T = \{t_1, t_2, \ldots, t_{N_T}\}$ is executed by a group of satellites $S = \{S_1, S_2, \ldots, S_{N_s}\}$. The observation tasks have multiple visible time windows $w = \{w_{t1}, w_{t2}, \ldots, w_{t_{N_T}}\}$ under a certain satellite resource that is capable of performing observations on multiple satellites at different moments of the visible time windows.

The MSIMP scenario is shown in Figure 1. The moving trajectory of the satellite at different moments is displayed on the orbit. The observation mission t_2 has multiple visible time windows, which can be simultaneously observed by satellite S_1 and satellite S_2 at time T_2. Satellite S_1 can observe $\{t_4, t_2, t_5\}$ respectively at time $\{T_1, T_2, T_3\}$ of the visible time window. Satellite S_2 can observe $\{t_1, t_2, t_3\}$ respectively at time $\{T_1, T_2, T_3\}$ of the visible time window. Constrained by satellite resources and its own maneuvering performance, each observation task is carried out by satellite resources only once. The time of any two execution tasks does not overlap for the same satellite and the execution time interval must be within the conversion time of satellite operation. According to the objective function and constraints, the MSIMP scheme is formulated for each observation mission under the condition of satisfying the constraints of multi-satellite imaging, with the goal of maximizing the comprehensive benefit of satellite imaging.

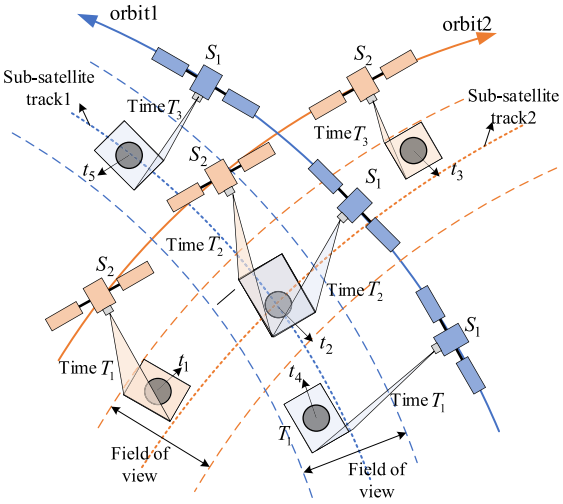

FIGURE 1. Schematic diagram of the basic process of MSIMP.

B. DIFFERENTIAL EVOLUTION ALGORITHM

The differential evolution algorithm (DE) is an intelligent optimization algorithm that is both robust and efficient, which has been widely used in many fields such as multi-agent planning systems and intelligent mission system control [28], [29]. Classical DE has two stages: population initialization and evolutionary iteration. The population generates N_P eligible individuals at random within the boundaries during the population initialization phase. During the population evolution phase, the loop is repeated for each generation of individuals, following the pattern of mutation, crossover, and selection until the end of the algorithm. The DE algorithm is shown in Figure 2.

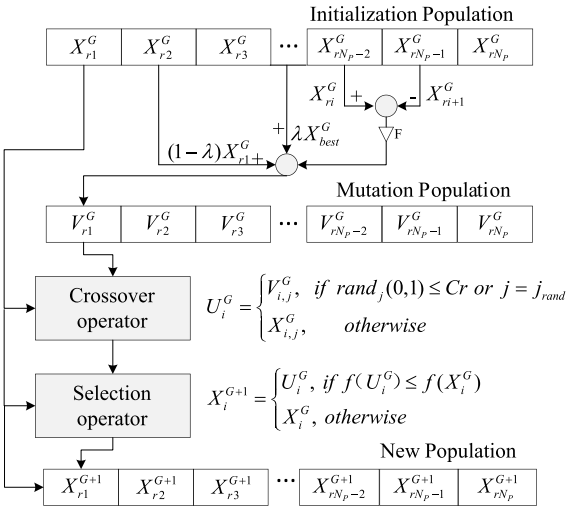

FIGURE 2. Schematic diagram of differential evolution algorithm.

1) INITIALIZATION OF THE POPULATION

In the population initialization phase, the upper and lower bounds of the parameter vector are determined, and N_P D-dimensional individuals are generated randomly and uniformly within the boundaries using a random generator:
where x_U^j, x_L^j are the upper and lower bounds of the j-th dimensional individual, respectively. $rand(0, 1)$ is a random number with a uniform distribution in the interval (0, 1).

2) MUTATION STRATEGY

The target vector X_i^G is generated by multiplying the random mutation factor V_i^G with the difference of the vector of adaptive distributions based on different difference mutation strategies. The current common differential mutation strategies are shown in equations (1)-(5)

(1) DE/RAND/1

$$V_i^G = X_{r_1}^G + F \cdot (X_{r_2}^G - X_{r_3}^G) \tag{1}$$

(2) DE/RAND/2

$$V_i^G = X_{r_1}^G + F \cdot (X_{r_2}^G - X_{r_3}^G + X_{r_4}^G - X_{r_5}^G) \tag{2}$$

(3) DE/BEST/1

$$V_i^G = X_{best}^G + F \cdot (X_{r_1}^G - X_{r_2}^G) \tag{3}$$

(4) DE/BEST/2

$$V_i^G = X_{best}^G + F \cdot (X_{r_1}^G - X_{r_2}^G + X_{r_3}^G - X_{r_4}^G) \tag{4}$$

(5) DE/CURRENT TO BEST/1

$$V_i^G = X_i^G + F \cdot (X_{best}^G - X_i^G + X_{r_1}^G - X_{r_2}^G) \tag{5}$$

where $X_{r_1}^G, X_{r_2}^G, X_{r_3}^G, X_{r_4}^G$ are randomly chosen individuals in the population that are different from X_i^G and satisfies the $r_1 \neq r_2 \neq r_3 \neq r_4 \neq i$; X_{best}^G denotes the best individual in generation 'G'. The parameter F is the mutation scaling factor.

3) CROSSOVER STRATEGY

To generate the experimental vector, the mutation vector is binomially crossed with the target vector, is shown as follow:

$$U_i^G = \begin{cases} V_{i,j}^G, & if\ rand_j(0,1) \le Cr\ or\ j = j_{rand} \\ X_{i,j}^G, & otherwise \end{cases} \tag{6}$$

where Cr is the cross operator on the interval [0,1].

4) SELECTION STRATEGY

The DE algorithm adopts a greedy strategy for the selection of the mutation vector and the target vector, the most optimal one enters the subsequent generation. The mathematical expression of the selection operation is presented in (7):

$$X_i^{G+1} = \begin{cases} U_i^G, & if\ f(U_i^G) \le f(X_i^G) \\ X_i^G, & otherwise \end{cases} \tag{7}$$

The classical DE adopts one-to-one greedy selection, in which the process of selection operation has an impact on the evolutionary direction of the entire population. In equation (7), $f(x)$ is the fitness value function and the higher fitness value vector enters the next generation.

III. PROBLEM DESCRIPTION

First, the MSIMP unified model based on task priority is introduced in this section. Second, the mathematical description of the unified model, objective function, constraints, and evaluation indicators is given.

A. THE MSIMP UNIFIED MODEL BASED ON TASK PRIORITY

This section builds a unified model based on two scenarios: large-scale imaging missions and emergency assurance tasks, and then chooses a mission assignment framework adaptively based on mission priority. In two types of scenarios, the observation process using the task priority-based MSIMP unified model can be described as follows:

First, due to the limitations of satellite resources and the requirements of different users' imaging tasks, the priority of MSIMP is quantified in a unified model based on imaging mission level according to the different imaging task level, task imaging type, urgency degree, and user level. An integer between [1] and [10] is used to set the priority of each target point, and the task priority is calculated as follows:

$$w = f(M_{level}, M_{type}, E_{\text{degree}}, U_{level}) \tag{8}$$

where equation (8) is a unified mathematical representation of the task priority effect factor. M_{level} is the imaging task level, M_{type} is the task imaging type, E_{degree} is the urgency degree, U_{level} is the user level.

$$A = \begin{bmatrix} A_{11} & A_{12} & \cdots & A_{1n} \\ A_{21} & A_{22} & \vdots & A_{2n} \\ \vdots & \vdots & & \vdots \\ A_{n1} & A_{n2} & \cdots & A_{nn} \end{bmatrix}, \quad A_{ij} = a_i / a_j \tag{9}$$

where equation (9) represents the task priority index judgment matrix, A_{ij} is the relative importance between index i and index j, a_i/a_j is the ratio of weight coefficients of index i and index j.

$$L = \sum_{i=1}^{n}\sum_{j=1}^{n}(A_{ij}a_j - a_i)^2 + 2\lambda\left(\sum_{j=1}^{n}a_j - 1\right) \tag{10}$$

where equation (10) represents the construction of the Lagrange multiplier method to solve a_j, λ is the undetermined coefficient.

$$w(X_1, X_2, X_3, X_4) = \sum_{j=1}^{n} a_j X_j \tag{11}$$

where equation (11) represents the calculation function of task priority influence factor, X_1, X_2, X_3, X_4 refers respectively to $M_{level}, M_{type}, E_{\text{degree}}, U_{level}$ in equation (8).

$$\text{Priority} = |w| \cdot 10, \quad \begin{cases} \text{Priority} \geq 7, & \textit{high priority} \\ 1 \leq \text{Priority} \leq 6, & \textit{low priority} \end{cases} \tag{12}$$

where equation (12) represents the calculation function of task priority. And it is divided into high priority (7-10 levels) and low priority (1-6 levels) to distinguish the importance of the target task.

Second, the proportion of high-priority tasks and low-priority tasks in total tasks is separately counted, and the mission assignment framework is adaptively selected based on the priority of each target in the user's proposed mission requirements. There are two types of allocation framework in the MSIMP mission assignment framework: large-scale imaging mission allocation framework and emergency assurance mission allocation framework. The large-scale imaging mission allocation framework is chosen for a set of missions that contain a greater proportion of low-priority missions than high-priority missions. In contrast, the emergency support mission allocation framework is chosen.

Finally, the MSIMP problem is transformed into a constraint satisfaction problem, and two optimization objectives and constraints for two types of assignment frameworks are proposed, namely, maximum mission benefit and minimum average response time for large-scale imaging missions and emergency support missions, respectively. The MSIMP based on UPM-IADE is used to achieve the optimization objective of maximum mission benefit and minimum response time.

Figure 3 depicts the observation process of the MSIMP unified model using a large-scale imaging mission scenario as an example. Black circles represent low-priority ground target points, blue circles represent high-priority ground target points, grey areas represent the satellite's field of view coverage, yellowish areas represent local areas containing target points, and blue dashed lines within the field of view indicate the track of subsatellite point.

In Figure 3, the circular arcs depict the satellite field of view and the lateral swing angle. The rectangular area at the bottom of the figure represents the mission satellite's observation time window in a single orbital circle, which is used to specify the visible relationship between the mission satellite and the target point, which is represented by a 6-tuple consisting of the target number, imaging start time, imaging end time, imaging duration, target priority, and side swing angle.

Because the proportion of low-priority target points is greater than the proportion of high-priority target points, the process of satellite earth observation in the framework of large-scale imaging missions using the MSIMP unified model based on task priority can be summarized as follows: High-speed imaging satellites in operational orbit select the appropriate mission assignment framework based on the imaging requirements of the user, assigning one or a group of imaging targets to multiple satellites that meet maneuverability constraints such as lateral swing angle and satellite imaging duration. Then, on the basis of the optimal objective assignment, a monorail task synthesis method based on visible time windows combined with an improved adaptive differential evolution algorithm is used to develop a task planning scheme that results in the optimal value of the overall optimization objective function.

B. ESTABLISH MSIMP OBJECTIVE FUNCTIONS AND CONSTRAINTS

1) MATHEMATICAL DEFINITIONS

The following mathematical definitions and decision variables are included in the MSIMP unified model based on task priority proposed in this work:

(1) Satellite mission set is $S = \{S_1, S_2, \ldots, S_{N_s}\}$, and the satellite number is N_S, where $\forall S_j \in S$, The relevant parameters include: maximum roll angle of remote sensor A_j, field angle of view θ_j, maximum uptime of satellite $t\max_{sj}$, minimum uptime of satellite $t\min_{sj}$, average angular velocity w_j, type of satellite payload d_j, orbit cycle number in the planning period N_j^o, and optimal image resolution of the satellite remote sensor r_j^s.

(2) In the MSIMP, the observation task set is $T = \{t_1, t_2, \ldots, t_{N_T}\}$,$N_T$ is the total number of tasks, where $\forall t_i \in T$. The relevant parameters include: $P_i = (P_i^{lat}, P_i^{lon})$, which indicates the position of task targets. P_i^{lat} and P_i^{lon} are the latitude and longitude of the target, respectively. The priority of the task is N_T. The operation mode of the satellite mission is T_i, which indicates that the side view for optical imaging satellites can be regarded as the working mode of earth observation and the working mode for the SAR imaging satellite is the imaging mode adopted by the satellite radar sensor. A minimum resolution r_i^t is required. In terms of $\forall t_i \in T$, we assume that the moment for the proposed requirements is t_i^S, and the response time of task t_i is $t_i^r = t_i^S - t_i^P$.

(3) The visible time windows for the earth observation task set T are calculated. Every visible time window of each

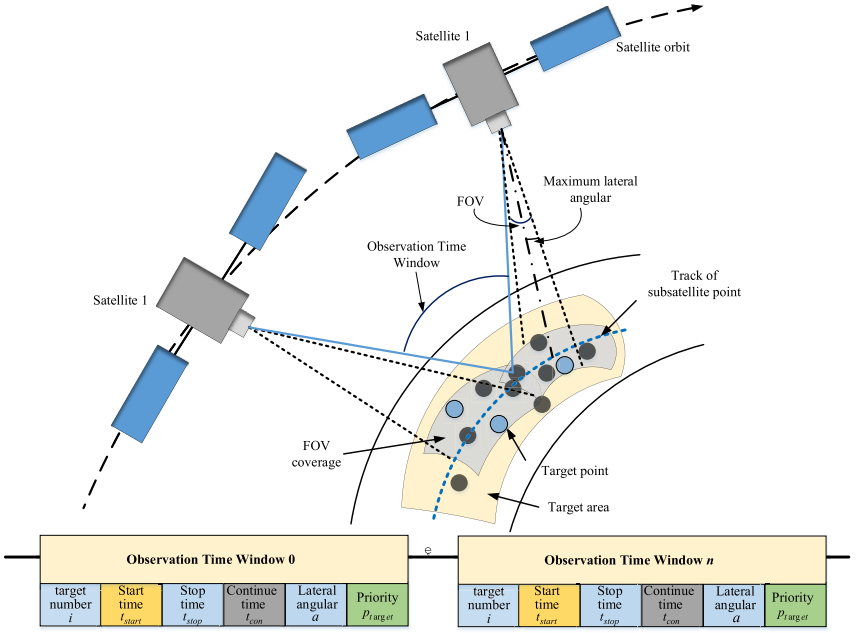

FIGURE 3. Demonstration of imaging satellite earth observation and illustration of the observation window.

imaging satellite comprises mission planning meta-tasks. The time window w_{ijk}^t of imaging satellite S_j to task t_i in orbit cycle k is: $w_{ijk}^t = \{i, j, k, t_{start}, t_{stop}, a\}$. Variable i represents the number of tasks, and j is the number of satellites. t_{start} and t_{stop} represent the start and end times of the visible time window, respectively. a represents the satellite mission lateral angular.

(4) After the calculation of the visible time window, the time window for the current satellite to execute its mission within a single orbital revolution can be defined as: $W_S = \{i, t_{start}, t_{stop}, t_{con}, a, p_{t\,\arg et}\}$. t_{con} indicates the imaging duration and $p_{t\,\arg et}$ indicates the task point priority.

(5) The meta-task sequence for the kth orbital revolution of satellite S_j is $M_{jk} = \left\{m_1^{jk}, m_2^{jk}, \ldots, m_{n_{jk}}^{jk}\right\}$ where n_{jk} is the number of meta-missions S_j performed during its kth orbit. The meta-task is synthesized, which task number is greater than one and satisfies the constraint condition. The task sequence after task synthesis is $C_{jk} = \left\{c_1^{jk}, c_2^{jk}, \ldots, c_{N_{jk}}^{jk}\right\}$. The single meta-task is also regarded as a synthesis task in this sequence. N_{jk} represents the number of synthesis missions in orbit k of satellite S_j. In $\forall c_P^{jk} \in C_{jk}$, the relevant parameters include: start time of synthetic tasks b_P^{jk}, end time of synthetic tasks e_P^{jk}, and roll angle of synthetic tasks a_P^{jk}.

(6) Decision variable.

$$x_{ijk} = \begin{cases} 0, & \text{not executed task} \\ 1, & \text{executed task} \end{cases} \tag{13}$$

where x_{ijk} is a 0–1 binary decision variable is used to describe the mission implementation situation. When $x_{ijk} = 0$, it represents that task t_i is not selected for execution. When $x_{ijk} = 1$, it indicates that task t_i is executed.

2) OBJECTIVE FUNCTIONS AND CONSTRAINTS

The objective function is defined for two different imaging requirements for large scale imaging mission and emergency support mission, according to the mission optimization objective elements. The mission completion rate is required for large-scale imaging missions. However, the task's timeliness is inadequate. Meanwhile, an emergency support mission is essentially a request for mission response time and mission completion rate in emergency situations.

a: OBJECT FUNCTIONS

- Mission significance optimization object functions:

$$\max : f_1(x_{ijk}) = \sum_{i=1}^{N_T} \sum_{j=1}^{N_S} \sum_{k=1}^{N_j^o} x_{ijk} w_i \tag{14}$$

where equation (14) states that this type of mission should maximize the sum of all task priority weights w_i. Imaging satellites should perform as many important earth observation tasks as possible.

- Mission effectiveness optimization object functions:

$$\min : f_2(x_{ijk}) = \frac{\sum_{i=1}^{N_T} \sum_{j=1}^{N_S} \sum_{k=1}^{N_j^o} x_{ijk} t_i^r}{N_T^S} \tag{15}$$

The optimization objective of this type of task requires the shortest average response time of the emergency support task.

Equation (15) represents the sum of the response times t_i^r for all tasks, taking the minimum average value for the number N_T^S of emergency support tasks.

b: CONSTRAINTS

Various constraints must be met in order for the objective function to be realized. For multi-satellite collaborative imaging task planning, the following constraints are abstracted from aspects of user requirements, collaborative tasks, and satellite resource constraints:

- Constraints of observation duration:

$$\forall j \in S, \quad \forall i \in T, \ \forall k \in W_{ijk}$$
$$x_{ijk} t\min_{S_j} \le x_{ijk}(e_p^{jk} - b_p^{jk}) \le x_{ijk} t\max_{S_j} \tag{16}$$

In equation (16), the minus between the imaging end time e_p^{jk} and the imaging start time b_p^{jk} of any of the planning element tasks in the mission synthesis sequence C_{jk} must be less than the maximum uptime of satellite $t\max_{s_j}$ and larger than the minimum uptime of satellite $t\min_{s_j}$.

- Constraint of working mode:

$$\forall w_{ijk}^t, \quad T_i = t_j \tag{17}$$

Equation (17) is the constraint of working mode. Each satellite payload is regarded as a mode of working. Satellites should meet within visible time windows, which are required the type of use of the remote sensor is consistent with current user needs.

- Constraint of resolution:

$$\forall w_{ijk}^t, \quad r_j^s \le r_i^t \tag{18}$$

Satellites can only carry out mission requests that fall within their scope of observation. As a result, the satellite S_j must meet the minimum resolution of the satellite remote sensor r_j^s that is less than or equal to the user's imaging requirement during any time window of the kth orbital circle task t_i.

- Constraint of satellite's lateral angular:

$$\forall c_p^{jk}, \quad \left|a_p^{jk}\right| \le A_j \tag{19}$$

During the ground observation process, the satellite should adjust the side swing angle based on the location of the ground target point for imaging, and if the ground target point is outside the track of the subsatellite point, the satellite should adjust the imaging side angle for observation. As shown in equation (19), satellite maneuverability requires that the imaging side angle of the ground target a_p^{jk} not exceed the satellite's maximum side angle A_j.

- Constraint of the lateral angular transition time:

$$\forall c_p^{jk}, \quad \left|a_p^{jk} - a_{p-1}^{jk}\right| / w_j \le b_p^{jk} - e_{p-1}^{jk} \tag{20}$$

For any of the planning tasks in the task synthesis sequence, the lateral angular transition time must be less than or equal to the observation duration.

- Constraint of uniqueness:

$$\forall t_i \in N_T, \quad \sum_{i=1}^{N_T} \sum_{j=1}^{N_S} \sum_{k=1}^{N_j^\sigma} x_{ijk} \le 1 \tag{21}$$

Equation (21) is uniqueness constraint, which indicates that the satellite sensor can only execute one task at a single time due to the constraint of satellite load.

c: EVALUATION INDICATORS

The mission evaluation indicators planned for multi-satellite imaging missions are as follows:

- Ideal benefit:

$$I_P = \sum_{i=1}^{N_T} w_i \tag{22}$$

Ideally, all target tasks are completed and the sum of the target priorities is the ideal benefit.

- Average benefit:

$$I_{aver} = \frac{\sum_{i=1}^{N_T} \sum_{j=1}^{N_S} \sum_{k=1}^{N_j^o} x_{ijk} w_i}{N_T} \tag{23}$$

The benefit of satellite execution target points averaged over all orbital circles.

- Mission benefit rate:

$$R_I = \frac{\sum_{i=1}^{N_T} \sum_{j=1}^{N_S} \sum_{k=1}^{N_j^o} x_{ijk} w_i}{\sum_{i=1}^{N_T} w_i} \cdot 100\% \tag{24}$$

The total benefit of the current mission as a percentage of the ideal benefit.

- Mission completion rate:

$$R_C = \frac{N_{Total}}{N_T} \cdot 100\% \tag{25}$$

The total number of target missions completed for this mission planning as a percentage of the total number of missions.

- Average mission response time:

$$Et_i^r = \frac{\sum_{i=1}^{N_T} \sum_{j=1}^{N_S} \sum_{k=1}^{N_j^o} x_{ijk} t_i^r}{N_T^S} \tag{26}$$

Equation (26) indicates the average response time of the executed mission.

IV. DESIGN OF UPM-IADE ALGORITHM

This section first describes the calculation of visible time window, then describes the monorail task synthesis method based on visible time windows, and finally introduces the MSIMP-based adaptive differential evolution algorithm.

A. VISIBLE TIME WINDOW CALCULATION

The MSIMP problem is classified as a mission planning problem with a time window. Satellite imaging missions have multiple visible time windows, and each visible time window is a satellite imaging mission planning meta-task with the satellite and the ground observation target. As a result, in the pre-processing phase of satellite imaging mission planning, the visible relationship between the mission satellite and the specified target point should first be clarified.

The visible window calculation can be used to generate the set of visible time windows between the execution task and the target point for a pre-defined multi-satellite mission planning scenario, as shown in Algorithm 1. First, the stkInit interface function is used to capture the path of each satellite and satellite-borne remote sensor, and then the satellite resource set S and satellite mission set T are obtained and saved to the database, containing information such as the maximum lateral swing angle and the track of subsatellite point data.

Second, the vertical foot position of the subsatellite point track is calculated using the latitude of the starting and ending positions of the observed target point. The position relationship between the observation target point and the track of the subsatellite point is determined, and the satellite's lateral swing angle is computed. Finally, the visible time windows that did not meet the resolution and working mode constraints are removed. Meanwhile, the visible time window of each target and associated parameters are saved.

Algorithm 1 Visible Window Algorithm Framework

Input: Satellite mission set S, Observation mission set T.
Output: Visible window w_{ijk}.

```
/* Use the stkIint to evaluate the visible window */
for j=1:length(SensorPaths)
for i=1:TargetNumber
    if ∀w^t_ijk, T_i = t_j;
    access(i,j).ComputeAccess;
Save the satellite resource set S and Observation mission set T data to the database;
    end if
end for
/*Calculate the lateral view */
for j=1:SatelliteNumber
    for i=1:TargetNumber
        midlat(i,j) = Startlat(i,j) / Stoplat(i,j);
    if tarlat(i) > midlat(i)
        aerEle(i,j) = 90 − aerEle(i,j);
    else if
        aerEle(i,j) = aerEle(i,j) − 90;
    end for
Remove the time windows that do not comply with the resolution and payload restrictions;
Save time windows w_ijk;
end for
end
```

B. MONORAIL TASK SYNTHESIS METHOD BASED ON VISIBLE TIME WINDOWS

The visible time window calculations as above clarify the visible relationship between the executing satellite and the target point, and this subsection investigates monorail task synthesis method based on visible time windows.

The resources, time, and angle of satellite observation for each meta-task are specified by calculating the visible time window. It means that each meta-task is an optional observation activity for mission execution, and mission planning is essentially the process of selecting and allocating meta-tasks. The imaging satellite combines multiple meta-tasks that satisfy certain conditions and have a temporal relationship to generate a mission synthesis and develop an imaging satellite mission planning scheme to achieve optimized objectives. This section considers synthetic tasks that include point targets, with the objective of optimizing the task of observing targets by adjusting the side view of the imaging satellite to simultaneously incorporate multiple point targets into the observation strip at the same time.

The following is the basic process of the monorail task synthesis method based on visible time windows. First, we go through all of the orbits and use the bubble method to sort the meta-tasks of each satellite's single orbit based on the observation time. The set of meta-task sequences for the kth orbit of satellite s_j is $M_{jk} = \left\{m_1^{jk}, m_2^{jk}, \ldots, m_{njk}^{jk}\right\}$, which is used to record the task information of all orbits that contain field of view, average lateral angular, and maximum uptime. Second, we consider task synthesis for multiple meta-tasks within a single orbital circle. The number of meta-tasks N_{jk} and side swing angle information a_i within the coverage range of the synthetic task angle are recorded in the meta-task sequence set that meets the conditions. Furthermore, the swing angle data is sorted ascendingly to generate a series of swing angles $A = \{a_1, a_2, \ldots, a_n\}$. Finally, the synthesis mission's observation angle a_i^m is calculated, the coverage of the synthetic angle and the task number s are determined, and the maximum benefit I_i^{jk} of the synthesis task c_i^{jk} is calculated. Algorithm 2 depicts the algorithm framework.

C. ADAPTIVE DIFFERENTIAL EVOLUTIONARY ALGORITHM

The adaptive differential evolution algorithm (ADE) is a widely used intelligent optimization algorithm whose performance is limited primarily by exploratory and exploitative aspects. A reasonable trade-off between the spatial search performance and exploitation performance is required to improve the performance of the algorithm and approach the optimal solution [30]. The ADE provides the flexibility to adjust algorithm parameters and alternate multiple mutation strategies during the optimization process based on the interrelationship between each generation of individuals and the optimal fitness value of individuals [31]. At the beginning of evolution, as the individual approaches the optimum, the control parameters become progressively smaller, which ensures a rapid approximation of the individual to the optimum. The

Algorithm 2 Monorail Mission Synthesis

Input: Field angle of view θ_j, average angular velocity w_j, target priority w_i, total track cycles I_t, all orbit numbers of synthesis missions N_{jk}, and lateral angular a_i.
Output: Synthetic task set c_{jk}.

```
for Total track cycles I_t
  if this orbital circle has observation missions
    M_jk = Bubble sort(m_l^jk);
    Save field of view, angular velocity, and max work time;
  end if
end for
for total track cycles I_t;
  if l > 1
    Determine the mission composition constraints;
      ∀c_p^jk, |a_p^jk| ≤ A_j;
      ∀c_p^jk, |a_p^jk − a_{p−1}^jk| / w_j ≤ b_p^jk − e_{p−1}^jk;
      Save information of N_jk,a_i;
      A = sort(a_i);
        for i = 1 to N_jk;
          a_i^m = a_i + θ_i/2;
          [max A_{a,b}^jk − θ_j/2, max A_{a,b}^jk + θ_j/2];
          I_{a,b}^jk = max(c_{a,b}^jk);
        end for
    end if
  end for
end
```

addition of random individual interaction in the late stage of evolution allows the algorithm to easily step outside the local optimum to improve global search capabilities, reducing tedious and time-consuming manual adjustments [32].

In this work, we propose a unified plan model and improved adaptive differential evolution algorithm. On the one hand, individual fitness values are considered as a reference factor for the spatial distribution of individuals, by calculating individual fitness values for each generation to assess whether the population satisfies the mutation requirements. Individuals in the UPM-IADE algorithm, on the other hand, are classified as ''exploitation,'' ''equilibrium,'' or ''exploration'' based on the individual weight ranking rule. Individuals adaptively choose mutation strategies from a pool of strategies in order to efficiently balance population diversity and convergence, overcoming the difficulty of having many MSIMP execution scenarios and long planning times.

1) INDIVIDUAL WEIGHT-RANK RULE

This section proposes a mutation operator based on the individual weight ranking rule that integrates individuals' fitness values and diversity contributions to strike a better balance between the exploratory and exploitative tendencies of differential evolutionary algorithms and search for an optimal solution for MSIMP in less time. Figure 4 depicts the algorithm's schematic diagram.

First, the fitness values of individuals in each generation of the population are presented. The individual fitness values are ranked in an ascending order and defined as the individual fitness value ranking.

$$R_{fit}^{i} = i, \quad i = 1, \ldots, N_P \tag{27}$$

where R_{fit}^{i} represents the individual's X_i^G fitness ranking. The ranking of individual fitness values is proportional to their size.

Second, fitness is a measure of survival advantage in each individual in the population. Individuals with large fitness values are primarily distributed around the local optimal solution or optimal individual in the spatial distribution. Individuals with small fitness values are randomly distributed at the edges of the space. Furthermore, the middle individual position in the spatial distribution between individuals with high fitness values and individuals with low fitness values. As reference values, the fitness values of middle individuals are chosen as follows:

$$fit_{middle} = fitness(R_{fitness}^{N_P}/2) \tag{28}$$

where $R_{fitness}^{N_P}$ represents the fitness value of the individual $X_{N_P}^G$. The individuals whose fitness values ranked as $R_{fitness}^{N_P}/2$ are defined as middle individuals. To some extent, the fitness value reflects the distribution of individuals in the population space. The difference in fitness between the current individual and the reference value can be roughly represented by the deviation value:

$$S = |fit_i - fit_{middle}|, \quad i = 1, \ldots, N_P \tag{29}$$

where fit_i denotes the fitness value of the current individual, S is the absolute value of the difference between the fitness values of the current and middle individuals.

If the deviation value S of individuals with large fitness values is large, then the current individual is far from the optimal individual or fall into the local optimum. Meanwhile, if individuals with small fitness values have large deviation values S, then the current individual is farther from the middle individual, and its position in space is more marginal. This situation can contribute more randomness and diversity to the exploration of solutions. Both these situations provide more information for searching the optimal solution.

The deviation values are sorted in ascending order, and the order of individuals is defined as diversity ranking shown as follow:

$$R_S^i = N_P - 1, \quad i = 1, \ldots, N_P \tag{30}$$

Then, the fitness value ranking and diversity ranking are weighted to determine each individual's final ranking, which is as follows:

$$R = w_F \times R_S^i + (1 - w_F) \times R_{fit}^i, \quad 0 < w_F < 1 \tag{31}$$

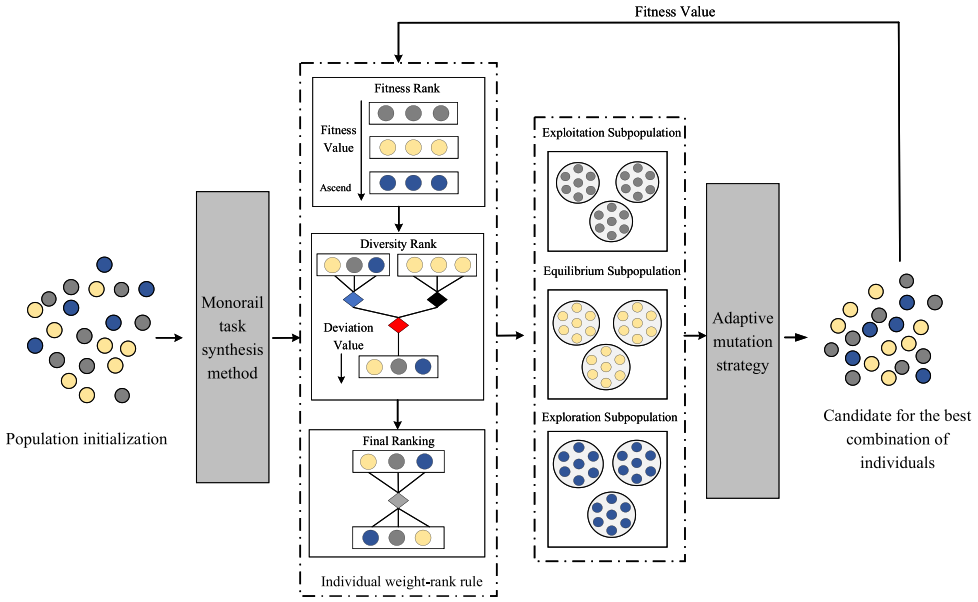

FIGURE 4. Individual weight-rank rule of UPM-IADE algorithm.

where R_S^i is the diversity ranking of the current individual X_i^G, and w_F is an important parameter that controls the evolutionary bias of the population.

$$w_F = \frac{fit_i^G}{fit_G^{\max}} \tag{32}$$

where fit_i^G is the fitness value of the current individual, and $fit_G^{\max}$ is the optimal fitness value in the current population. The weights w_F are dynamically adjusted based on the ratio of the current individual fitness value to the current population's optimal fitness value. The final fitness value ranking is generated by the weighted combination of the fitness value ranking and the diversity ranking, and it is used to select individuals that meet the variation requirements for the next generation. Finally, due to the long planning time of MSIMP, the population individuals meeting the mutation requirements are ranked based on the final fitness value. Each generation's population is divided into "exploitation" individuals, "equilibrium" individuals, and "exploration" individuals. The details are described in Algorithm 3.

2) ADAPTIVE MUTATION STRATEGIES POOL

In algorithm 3, the individual weight ranking rule is used to divide each generation of the population into three different types of individuals: "exploitation" individuals, "equilibrium" individuals, and "exploration" individuals. The strategies and basic properties are illustrated in Table 1.

"DE/best/1" mutation strategy uses the best individuals from the current population as the base vector, which can retain more excellent genes from the parent individuals. This strategy has a high degree of convergence. "DE/rand/1" in mutation strategy 2 randomly selects individuals in the generated vector from the population, which has a higher global search ability. In mutation strategy 3, "DE/current-to-best/1" can effectively balance the individual's exploration

Algorithm 3 Individual Weight-Rank Rule

Input: Population size N_P, Each individual's fitness value *fit*;
Output: Individuals Sorted Based on Weights, Three subpopulations;

1/*Fitness ranking* /
2 Access to Each individual's fitness values;
3 $R_{fit} = sort(fit)$;
4 $R_{fit}^i = i, i = 1, \ldots, N_P$;
5 /*Select reference values* /
6 $fit_{middle} = fitness(R_{fitness}^{N_P}/2)$;
7/*diversity ranking* /
8 $S = |fit_i - fit_{middle}|, i = 1, \ldots, N_P$;
9 $R_S = sort(S)$;
10 $R_S^i = N_P - 1, i = 1, \ldots, N_P$;
11/*Final ranking based on weights* /
12 $w_F = \frac{fit_G^i}{fit_G^{\max}}$;
13 $R = w_F \times R_s^i + (1 - w_F) \times R_{fit}^i, 0 < w_F < 1$;
14 Individuals ranking based on weights;
15 Dividing the population into three subpopulations;
16 ***end***

TABLE 1. Mutation strategy parameter setting.

Strategy	Parameters
DE/best/1	$F = 0.5, CR = 0.1$
DE/rand/1	$F = 1.0, CR = 0.9$
DE/current-to-best	$F = 0.8, CR = 0.5$

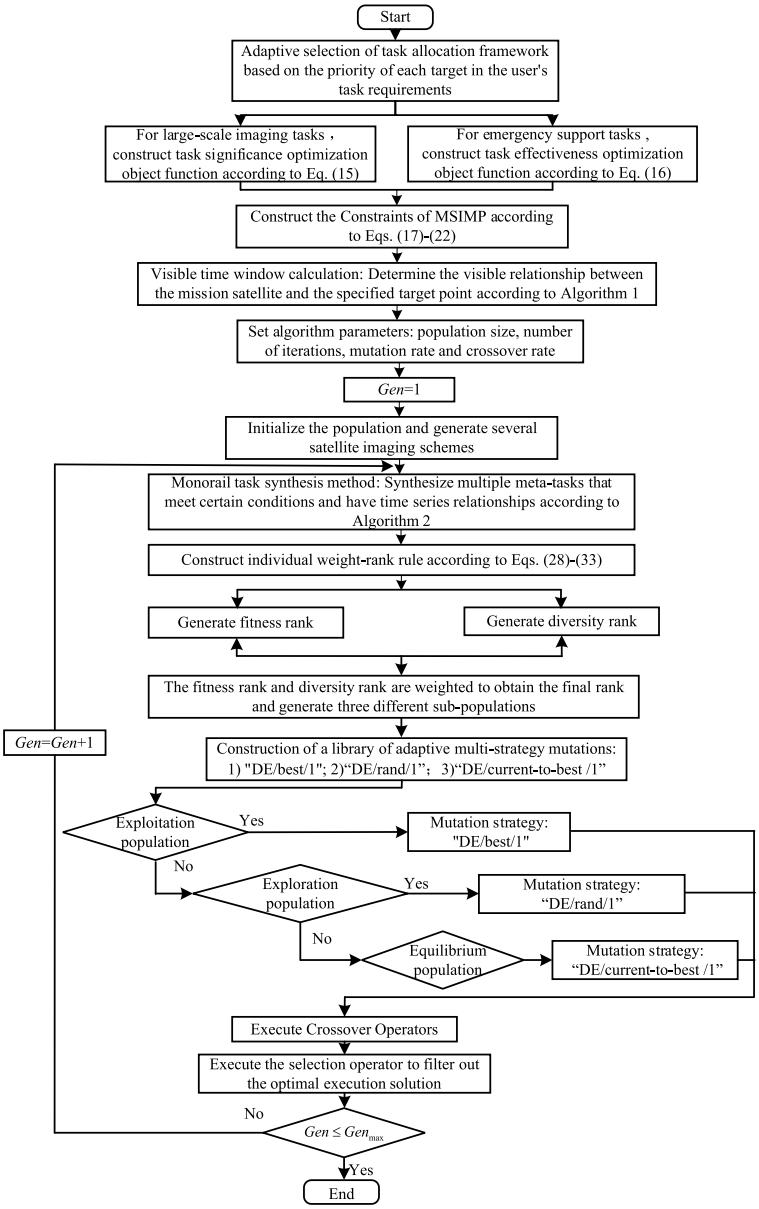

FIGURE 5. MSIMP flowchart based on UPM-IADE algorithm.

and exploitation. Furthermore, this strategy has the characteristics of strong global search ability and fast convergence to improve the algorithm's convergence speed. Individuals can choose mutation strategies from the adaptive mutation strategies pool based on their exploration and exploitation biases. As a result, the overall performance of the UPM-IADE algorithm is improved in two ways: identifying the optimal solution region of the vector solution space more effectively and accelerating optimization convergence. At each iteration, the adaptive mutation strategies pool contains only one set of mutation strategies.

3) FLOWCHART BASED ON UPM-IADE ALGORITHM

Figure 5 depicts the MSIMP flow chart based on the UPM-IADE algorithm, including the constraints and objective functions for constructing the MSIMP, as well as the principle of the adaptive differential evolution algorithm for the MSIMP.

V. EXPERIMENTAL SIMULATION, RESULT AND ANALYSIS

In this work, four groups of simulation experiments are carried out in Matlab2016a and STK11.6 software to validate the effectiveness of UPM-IADE-based MSIMP. Experiment 1: feasibility and stabilityfor a large-scale imaging mission on a global scale. Experiment 2: feasibility and stability for a local area-oriented emergency support mission. Experiments 3 and 4 compared the performance of the UPM-IADE algorithm to similar algorithms in two different types of planning scenarios.

TABLE 2. Satellite payload parameters and orbital parameters.

No.Sat	a / (km)	e / (°)	i / (°)	*RAAN*	ω / (°)	φ / (°)	θ_j / (°)	$t\max_{S_j}$ / (s)	A_j (°)	w_j / (°/s)	r_j^s / (m)
Sat1	7571.77	0.0013	100.418	244.74	354.34	118.23	6	400	40	0.3	2.5
Sat2	6882.45	0.0009	97.719	75.86	69.09	141.91	6	400	40	0.3	2.5
Sat3	7012.33	0.0040	97.824	244.92	59.34	177.50	6	450	40	0.3	2
Sat4	6869.10	0.0011	97.205	177.82	160.05	237.09	6	450	40	0.4	2
Sat5	7583.60	0.0017	100.218	159.03	95.89	93.60	7	450	45	0.4	1.5
Sat6	6862.79	0.0020	97.379	266.41	115.24	184.37	7	450	45	0.4	1.5
Sat7	6999.83	0.0019	98.140	124.36	117.39	188.44	8	500	45	0.5	1.5
Sat8	7022.88	0.0027	98.138	166.39	53.26	330.9	8	500	45	0.5	1.5

A. EXPERIMENTAL DESIGN

Each demonstration scenario is built using STK software and eight imaging satellites chosen from the STK standard database. In order to conserve satellite resources, the maximum side-swing angle for each satellite is limited to 40°.

Six orbital elements can be used to determine the position of imaging satellites: Semi-major axis (a), eccentricity (e), orbital inclination (i), argument of perigee (ω). right ascension of the ascending node (*RAAN*), and true anomaly (φ). The satellite payload parameters include the following: field angle of view (θ_j), maximum uptime of the satellite ($t\max_{S_j}$), maximum roll angle of the remote sensor (A_j), average angular velocity, and optimal image resolution of the satellite remote sensor (r_j^s). The number of orbital elements and satellite payload parameters of each satellite are shown in Table 2.

In this study, we employ similar algorithms and the UPM-IADE algorithm for comparison experiments to evaluate the feasibility and stability of the UPM-IADE Algorithm. Differential Evolution Algorithm (DE) and Self-Adaptive Differential Evolution Algorithm (SADE) are two similar algorithms. The DE algorithm sets the mutation scaling factor $F = 0.3$, Crossover rate $CR = 0.5$; The initial value of SADE algorithm mutation scaling factor is set to $F = 0.5$, the initial crossover rate is set to $CR = 0.5$.

B. VALIDATION EXPERIMENTS

1) EXPERIMENT 1: FEASIBILITY AND STABILITY FOR A LARGE-SCALE IMAGING MISSION ON A GLOBAL SCALE

Large-scale imaging missions are mostly routine tasks that should be observed on specific space locations and targets on a regular basis based on mission requirements, and imaging satellites should complete as many imaging tasks as possible. This experiment used a uniformly distributed pattern of 100 imaging target points to simulate the user mission requirements within a global range of latitude [−30,70] and longitude [−180,180]. Figure 6 depicts the distribution of target points to be observed within the global range.

It is worth noting that the geographical location of the target point influences the mission's synthetic observation. To reduce errors caused by target point distribution, the geographical distribution of target points is set in a uniformly distributed pattern using the method used by Cui et al. to construct problem instances [33].

The population size of the UPM-IADE algorithm is set to 200, and the maximum number of iterations is set to 300. Table 3 shows the optimal assignment results for MSIMP, where "Sat" refers to the satellite allocation sequence, "Target" refers to the target point allocation sequence, and "Ptarget" refers to the target mission execution priority. The symbol "−" indicates that the time window assigned to this target point does not satisfy the resolution and load constraints, and thus no imaging task is scheduled.

Table 3 analyzes the allocation of mission satellites to target points based on the MSIMP optimal allocation results. Figure 7(a) clearly shows the execution target point numbers and corresponding target point priority for the eight satellites in the large-scale imaging scenario. In Figure 7 (a), the x-axis represents the target task number, the y-axis represents the execution priority of the corresponding target task, and the z-axis represents the execution task satellite number. To clarify the execution of various satellites, eight different colored squares are used to represent the target tasks of various satellites. In Figure 7(b), priorities 1-10 in the legend are used to respectively indicate the ratio of activities of each priority to all required tasks in a large imaging mission experiment. Figure 7(b) shows that among the 100 requirement tasks, unexecuted tasks accounted for 10% of the total number of required tasks, and tasks with a priority of less than 6 accounted for 53% of the total number of required tasks, with satisfactory results.

The simulation results above demonstrate that the UPM-IADE algorithm proposed in this paper can effectively solve the planning model in large-scale mission scenarios and deal with the satellite and target point assignment relationship. As a result, MSIMP using the UPM-IADE algorithm is a highly feasible option

Table 4 shows the outcomes of multiple iterations of the large-scale imaging mission at various population sizes,

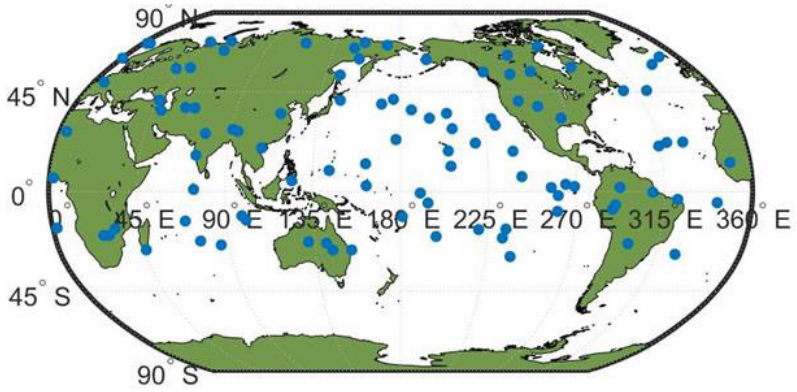

FIGURE 6. Large-scale imaging mission distribution.

TABLE 3. The simulated experiment results of common imaging mission planning.

Common imaging mission planning results																				
Target	1	2	3	4	5	6	7	8	9	10	11	12	13	14	15	16	17	18	19	20
Sat	5	-	5	8	8	3	3	6	4	6	8	-	1	3	4	2	3	-	5	5
Ptarget	5	-	3	5	6	1	8	3	10	6	3	-	8	4	2	2	9	-	2	7
Target	21	22	23	24	25	26	27	28	29	30	31	32	33	34	35	36	37	38	39	40
Sat	2	5	4	4	4	8	-	7	3	5	1	3	7	-	4	4	5	4	3	5
Ptarget	10	1	3	6	3	4	-	2	7	9	1	5	7	-	9	1	3	1	7	8
Target	41	42	43	44	45	46	47	48	49	50	51	52	53	54	55	56	57	58	59	60
Sat	5	4	3	8	7	4	6	5	-	2	6	7	6	2	1	5	-	3	3	8
Ptarget	6	7	4	9	7	4	4	33	-	3	6	3	10	7	5	3	-	1	6	7
Target	61	62	63	64	65	66	67	68	69	70	71	72	73	74	75	76	77	78	79	80
Sat	8	2	6	7	8	8	3	1	5	-	2	2	7	2	1	-	1	4	5	6
Ptarget	4	6	2	5	8	6	9	5	5	-	10	9	9	5	1	-	4	2	3	10
Target	81	82	83	84	85	86	87	88	89	90	91	92	93	94	95	96	97	98	99	100
Sat	6	7	1	2	2	3	1	6	-	7	5	2	7	1	3	1	2	5	3	7
Ptarget	8	3	2	8	1	2	1	5	-	1	4	9	9	4	5	10	5	2	5	4

including the ideal benefit value $Value_P$, average benefit value $Value_{aver}$, mission completion rate R_C, mission benefit rate R_I, and mission response time $Aver\_t_i^r$ for each population size, where *Num_Iter* is the number of experimental iterations and *Times* is the number of experimental repetitions.

The following conclusions can be drawn from the simulated experimental data in Table 4:

(1) The mission completion rate and mission benefit of using the UPM-IADE algorithm to solve the MSIMP problem have less difference as the number of populations and iterations increases, and the average benefit value is close to the ideal benefit. At a population size of 300 and 300 iterations, this instance achieves the optimal value of the optimization objective function, with an average gain of 464.01.

(2) Both the mission benefit rate and the mission completion rate exceed 90%, demonstrating that the final solution is feasible and satisfies the multiple mission constraints in the construction model, reflecting the collaborative nature of multi-satellite mission planning.

(3) Considering the UPM-IADE algorithm performance under parameter control, the average benefit value is close to the ideal benefit value for multiple iterations with different population sizes, demonstrating that the UPM-IADE algorithm search results are close to the global optimal solution.

In conclusion, the UPM-IADE algorithm-based MSIMP has strong stability.

2) EXPERIMENT 2: FEASIBILITY AND STABILITY OF EXPERIMENTS FOR LOCAL AREA-ORIENTED EMERGENCY SUPPORT MISSION

The emergency response requirements are mostly applied to urgent and unexpected situations, which place demands on

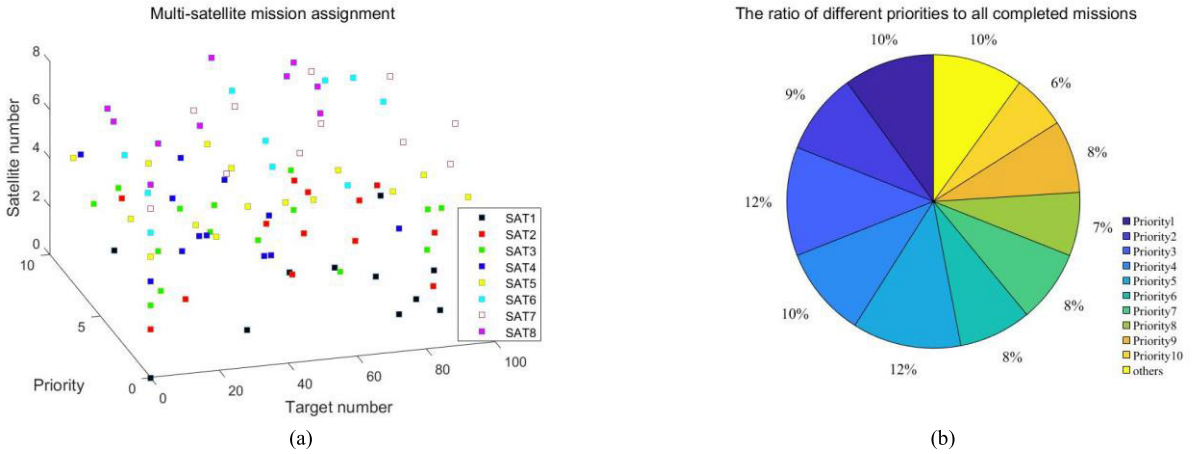

FIGURE 7. Result of large-scale imaging tasks. (a)multi-satellite mission assignment in large-scale imaging tasks diagram. (b)The ratio of missions with different priorities to large-scale imaging tasks.

TABLE 4. The result of different population sizes with Muti-iterations for the large-scale imaging missions.

N_p	Num_Iter	$Times$	$Value_F$	$Value_{aver}$	R_C (%)	R_I (%)	$Aver\_t_i^r$ (s)
100	100	10	480	440.01	91%	91.67%	140.4
	300	10	480	447.98	93%	93.33%	150.2
	500	10	480	432.00	90%	90.00%	155.8
	1000	10	480	440.49	91%	91.77%	162.6
200	100	10	480	444.96	92%	92.70%	145.5
	300	10	480	459.21	95%	95.67%	160.4
	500	10	480	448.17	93%	93.37%	163.3
	1000	10	480	450.38	93%	93.83%	165.6
300	100	10	480	448.17	93%	93.37%	155.3
	300	10	480	464.01	96%	96.67%	171.4
	500	10	480	458.97	95%	95.62%	176.9
	1000	10	480	459.93	95%	95.82%	196.8

the mission's importance and timeliness, as well as maximizing total tasks benefit and achieving the shortest average response time. This section simulates a natural disaster in a region, with 30 mission targets chosen at random as emergency support mission targets. The satellite continuously maps the affected area, allowing for the shortest average response time for all tasks. Figure 8 shows the distribution of the target points to be observed in the local area.

Table 5 depicts the task allocation relationships between satellites and target points for an emergency support mission with a population size of 200 and 300 iterations. Table 5 shows that the UPM-IADE algorithm proposed in this paper can effectively deal with the satellite and target point allocation relationship in emergency mission scenarios. As a result, MSIMP based on the UPM-IADE algorithm is feasible.

Table 6 presents the results of multiple iterations with different population sizes for ideal benefit values $Value_P$, average benefit values $Value_{aver}$, mission completion rates R_C, and mission response times $Aver\_t_i^r$ for each population size.

The following conclusions can be drawn from Tables 5 and 6:

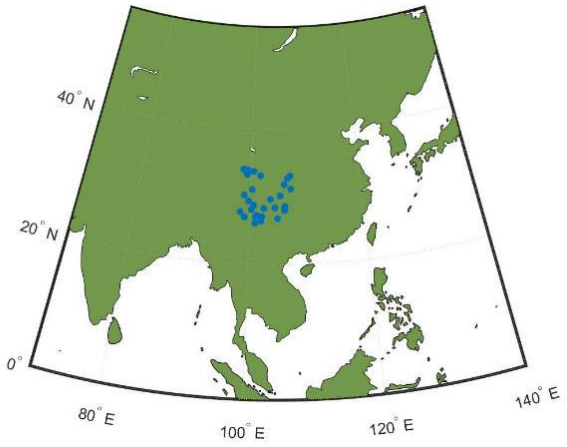

FIGURE 8. Emergency support mission targets distribution.

(1) When dealing with small-scale emergency support missions, the UPM-IADE algorithm achieves a small difference in mission completion rate and mission benefit rate, indicating good performance for multiple iterations of experiments with different population sizes.

TABLE 5. The simulated experiment results of emergency support imaging mission planning.

Emergency support imaging mission planning results															
Target	1	2	3	4	5	6	7	8	9	10	11	12	13	14	15
Sat	1	6	6	6	7	6	3	4	6	1	1	1	6	4	5
Target	16	17	18	19	20	21	22	23	24	25	26	27	28	29	30
Sat	5	6	5	1	3	5	5	1	6	4	3	3	7	5	8

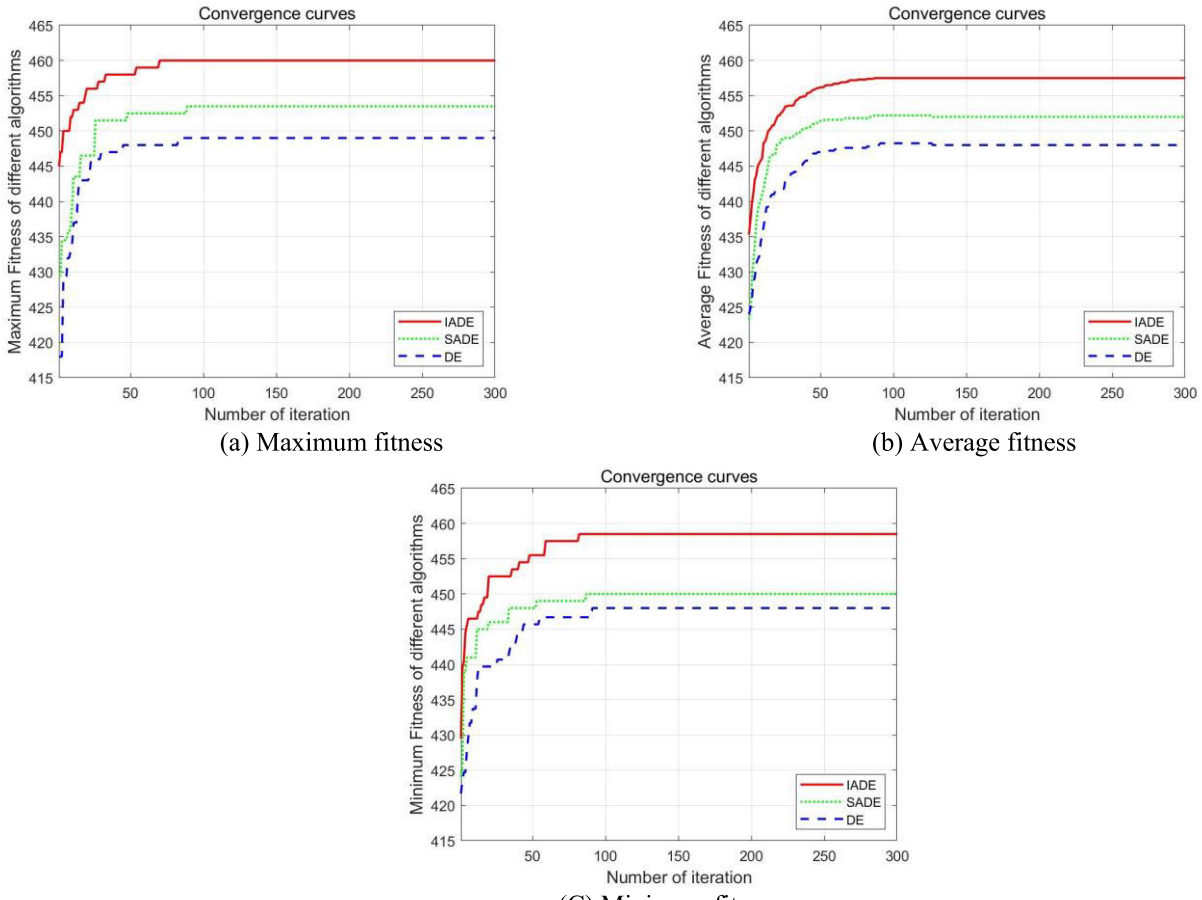

(a) Maximum fitness

(b) Average fitness

(C) Minimum fitness

FIGURE 9. Convergence curve of fitness value using different algorithms.

(2) In this instance, the average benefit values are all close to the ideal benefit values, indicating that the MSIMP solution using the UPM-IADE algorithm is close to the global optimal solution.
(3) The results of this experiment show that the system is capable of carrying out emergency missions well; As the number of iterations and population size increase, the response time increases, but the emergency support tasks are all well executed.
(4) Experiment 2 and Experiment 1 show that the population sizes adapted to the different instances differ. For the current instance, a population size of 200 is optimal, with an average benefit of 300 when the number of iterations is 300 and all target points are executed for the imaging mission.

Experiment 1 and Experiment 2 simulation results show that the UPM-IADE-based MSIMP proposed in this work can effectively solve the MSIMP problem. UPM-IADE validates the unified model's feasibility and stability in both large-scale imaging and emergency support mission scenarios, addressing the MSIMP mission allocation model's poor scalability and weak algorithm targeting in different mission requirements.

TABLE 6. Simulation experiment data analysis for the emergency support imaging mission.

N_p	Num_Iter	$Times$	$Value_P$	$Value_{aver}$	R_C (%)	R_I (%)	$Aver\_t_i^r$ (s)
100	100	10	300	291.7	97%	97.25%	39.16
	300	10	300	298.7	98%	99.58%	40.46
	500	10	300	293.1	97%	97.69 %	43.53
	1000	10	300	293.6	98%	97.88%	45.63
200	100	10	300	293.5	97%	97.83%	40.13
	300	10	300	300.0	100%	100%	43.00
	500	10	300	294.9	98%	98.33%	44.73
	1000	10	300	296.4	98%	98.80%	46.20
300	100	10	300	294.7	98%	98.25%	40.47
	300	10	300	295.4	99%	98.46%	42.50
	500	10	300	290.0	96%	96.67%	44.10
	1000	10	300	291.0	97%	97.50%	46.20

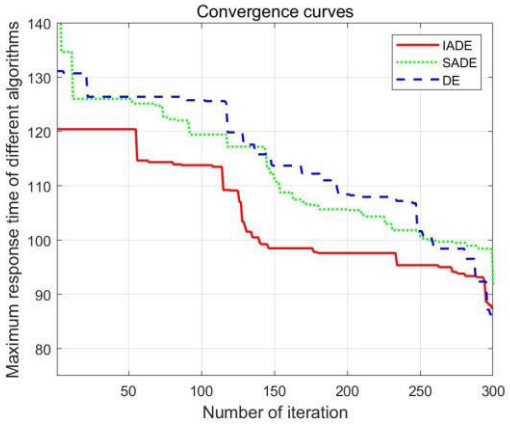

(a)Maximum response time

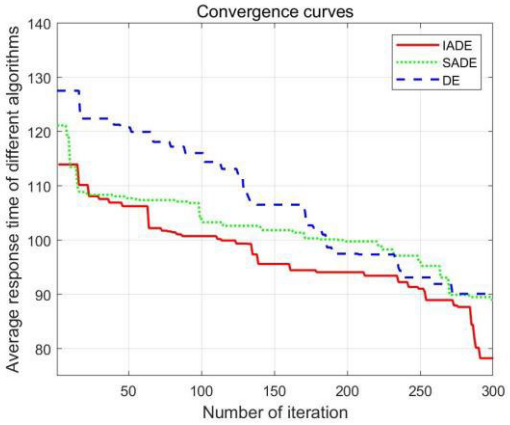

(b) Average response time

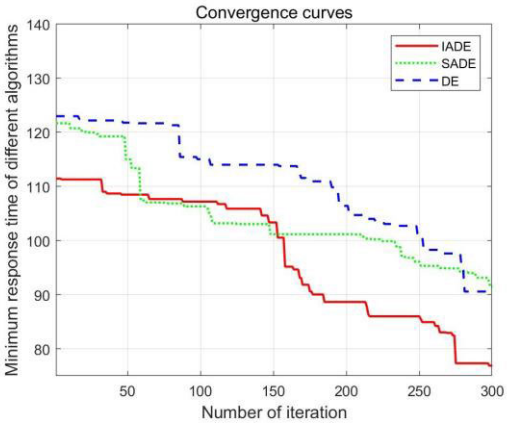

(C) Minimum response time

FIGURE 10. Convergence curve of response time using different algorithms.

C. COMPARISON OF UPM-IADE AND OTHER ALGORITHMS

To accurately assess the performance of the UPM-IADE algorithm and confirm its progress in terms of both the fitness value of the optimization objective and the effectiveness of optimization. In this section, the UPM-IADE algorithm is compared with the DE and SADE algorithms in the above two types of situations, the large-scale imaging mission and the emergency support mission, to further study how well it performs when solving MSIMP.

1) EXPERIMENT 3: LARGE-SCALE IMAGING MISSION WITH DIFFERENT ALGORITHMS

Compared experiments are carried out to validate the performance improvement of the UPM-IADE algorithm in terms of optimization mission benefit and optimization

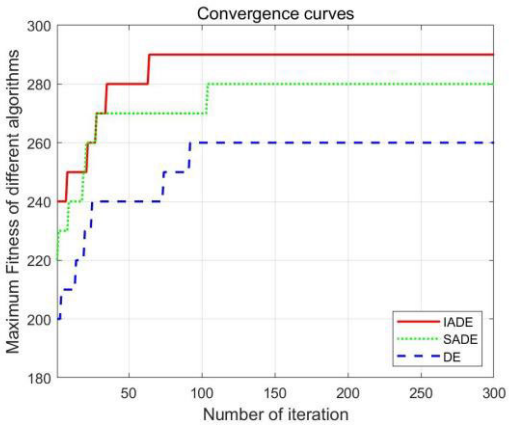

(a) Maximum fitness

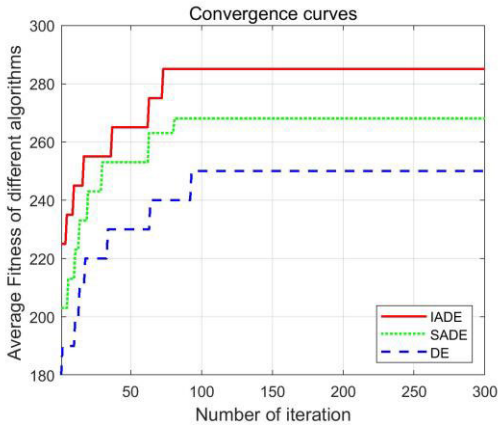

(b) Average fitness

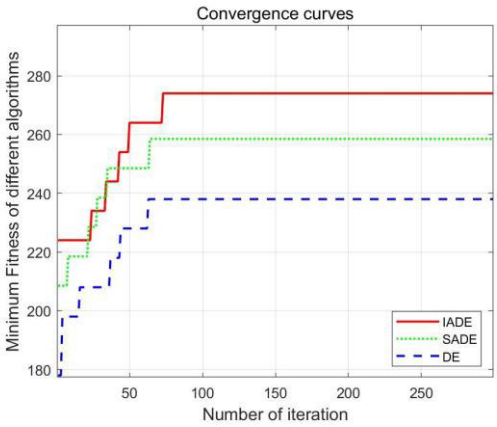

(c) Minimum fitness

FIGURE 11. **Convergence curve of fitness value using different algorithms.**

efficiency using three algorithms for a large-scale imaging mission scenario with a target point of 100, controlled by a parameter of population size 300 iteration count 300.

We chose six evaluation indexes to analyze the performance of the UPM-IADE algorithm in order to verify the performance improvement in terms of optimization target fitness value and optimization efficiency:

(1) Maximum fitness value: $I_{\max} = \max(\sum_{i=1}^{N_T}\sum_{j=1}^{N_S}\sum_{k=1}^{N_j^o} x_{ijk}w_i)$ represents the maximum mission benefit of the satellite executing the target within all orbital circles, where x_{ijk} is the decision variable of executing the task, w_i is priority of executing the task. This index reflects the ability of algorithms to optimize in different experiments.

(2) Average fitness value: $I_{aver} = \sum_{i=1}^{N_T}\sum_{j=1}^{N_S}\sum_{k=1}^{N_j^o} x_{ijk}w_i \Big/ N_T$ represents the average mission benefit of the satellite executing the target within all orbital circles, where N_T is number of tasks. This index reflects the stability of algorithms in different experiments.

(3) Minimum fitness value: $I_{\min} = \min(\sum_{i=1}^{N_T}\sum_{j=1}^{N_S}\sum_{k=1}^{N_j^o} x_{ijk}w_i)$ represents the minimum mission benefit of the satellite executing the target within all orbital circles. This index reflects the solution of the algorithm to the minimum benefit.

(4) Maximum response time: $T_{\max} = \max(\sum_{i=1}^{N_T}\sum_{j=1}^{N_S}\sum_{k=1}^{N_j^o} x_{ijk}t_i^r)$ represents the maximum response time t_i^r of all tasks x_{ijk}. This indicator reflects the maximum running time of the mission planning system.

(5) Average response time: $T_{aver} = \sum_{i=1}^{N_T}\sum_{j=1}^{N_S}\sum_{k=1}^{N_j^o} x_{ijk}t_i^r \Big/ N_T$ represents the average response time t_i^r of all tasks x_{ijk}. This indicator reflects the average running time of the mission planning system.

(6) Minimum response time: $T_{\min} = \min(\sum_{i=1}^{N_T}\sum_{j=1}^{N_S}\sum_{k=1}^{N_j^o} x_{ijk}t_i^r)$ represents the minimum response time t_i^r of all tasks x_{ijk}. This indicator reflects the minimum running time of the mission planning system.

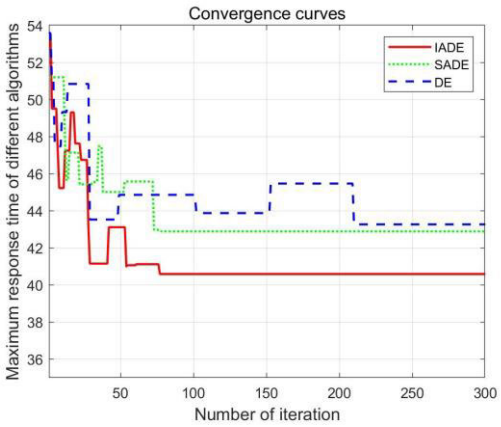

(a) Maximum response time

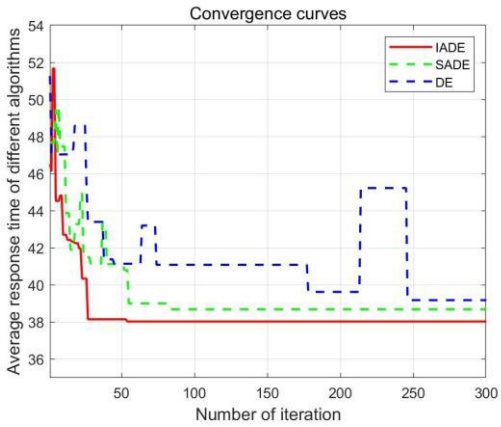

(b) Average response time

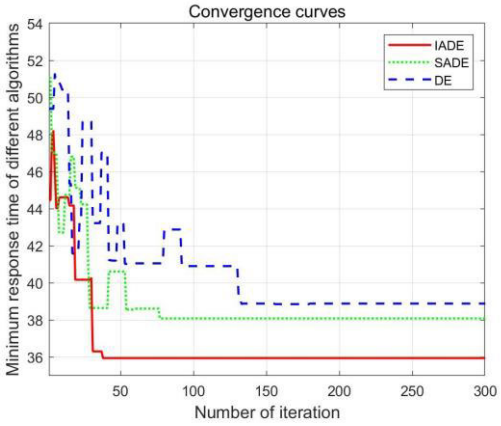

(C) Minimum response time

FIGURE 12. Convergence curve of response time using different algorithms.

The convergence curves of the maximum/average/minimum fitness values of the UPM-IADE, SADE, and DE algorithms are shown in Figure 9. In comparison to the SADE and DE algorithms, the UPM-IADE algorithm has significantly higher maximum, average, and minimum fitness values. The convergence curve of fitness values of the UPM-IADE algorithm converges to the approximate vicinity of the optimal solution in 65-74 generations, indicating a fast convergence rate in the early stages of the search. As a result, the UPM-IADE algorithm performs well in terms of convergence.

Figure 10 depicts the maximum/average/minimum response time convergence curves of the UPM-IADE, SADE, and DE algorithms. In Figure 10, the response times of the UPM-IADE algorithm are significantly less than those of the SADE and DE algorithms when the convergence curves of the maximum/average/minimum response times are compared. It demonstrates that the UPM-IADE method takes less time to execute than the SADE and DE algorithms in the MSIMP system, and the UPM-IADE algorithm can solve the optimal execution plan in a short time.

Figure 10(a) shows that the UPM-IADE algorithm enters the fast convergence stage between generations 120 and 140. The reason for this is that the UPM-IADE algorithm has sufficient exploration capability early on and can accelerate convergence speed when it explores the optimal solution region. It tends to develop fine search and enter fast convergence in the middle and late stages of the algorithm, indicating that the mutation operator based on weight sorting rule plays an important role in further improving the solution.

2) EXPERIMENT 4: LOCAL AREA-ORIENTED EMERGENCY SUPPORT MISSION WITH DIFFERENT ALGORITHMS

Algorithm performance comparison experiments are carried out in an emergency support mission scenario using the three algorithms mentioned above, UPM-IADE, SADE, and DE, with the parameters of each algorithm set to a population size of 200 iterations of 300. The convergence curves of the fitness values of the various algorithms are depicted in Figure 11.

Figures 11(a), 11 (b), and 11 (c) show the convergence curves in three indicators of each algorithm, namely maximum fitness, average fitness, and minimum fitness. In terms of optimization mission benefits, the three metrics of the UPM-IADE algorithm converged quickly within 65-74 generations, while the maximum fitness value, average fitness value, and minimum fitness value were significantly higher

than the SADE and DE algorithms. It is clear that the UPM-IADE algorithm performs well in terms of convergence.

Figure 12 represents the response time convergence curves for the different algorithms. Subpanels (a), (b), and (c) of Figure 12 depict the convergence curves of the three algorithms in terms of maximum response time, average response time, and minimum response time. Based on the evaluation of the three indicators, the response time of the IADE algorithm is shorter than that of the other algorithms in terms of optimal efficiency. As a result, the IADE algorithm's efficiency improves.

The following results can be obtained based on the above experimental results comparing the performance of the UPM-IADE algorithm with similar algorithms in two types of scenarios for large-scale imaging missions and local area-oriented emergency support missions. On the one hand, when applied to both types of scenarios, the UPM-IADE algorithm converges faster than similar algorithms in the fitness value convergence curve and achieves greater benefits in the fitness value when convergence is reached. This is significant proof that the mutation operator based on the individual weight ranking rule proposed in the UPM-IADE algorithm is essential.

On the other hand, the UPM-IADE algorithm has a shorter response time than similar algorithms in both types of scenarios. The experimental results show that this method ensure that the multi-satellite mission planning system solves for the optimal execution solution in a shorter time. The UPM-IADE algorithm significantly improves both optimization mission benefits and optimization efficiency.

VI. CONCLUSION AND FUTURE WORK

To solve the difficult problem of planning multi-satellite imaging missions, this paper proposes a unified plan model and an improved adaptive differential evolution algorithm. In terms of developing planning models: to avoid the difficult problems of inconsistent models and long planning times in mission planning for different user requirements, a unified model is constructed for the first time for two types of scenarios, namely large-scale imaging mission and emergency support mission, overcoming the problems of poor scalability of MSIMP models and weakly pertinent algorithms. In terms of mission planning algorithms, a monorail task synthesis method based on visible time windows is proposed to improve MSIMP execution efficiency due to weak satellite mobility and a limited number of imaging cycles in a single orbit. In terms of developing adaptive algorithms, we proposed a unified plan model and improved adaptive differential evolution algorithm, as well as a weight-ranking mutation rule, to effectively balance population diversity and convergence. This overcame the difficulty of multiple execution schemes and long planning time for MSIMP. The experimental results demonstrate that the algorithm can effectively solve both large-scale imaging mission and emergency support mission scenarios, and in addition, it has high mission benefit and a short response time when dealing with MSIMP.

Future research will focus on considering MSIMP in a dynamic environment. In a deterministic environment, the UPM-IADE proposed in this work can effectively solve the application problems of MSIMP in the two scenarios of large-scale imaging mission and emergency support mission. However, in the actual implementation process, multiple imaging satellites are frequently confronted with a large number of uncertain factors. For example, cannot deal with unexpected situations such as cloud occlusion, satellite equipment failure, and satellite resource failure in real time, which leads to the ineffective execution of satellite observation tasks. Therefore, it is necessary to carry out further research on MSIMP in a dynamic environment.

REFERENCES

[1] J. Chen, H. Tang, J. Ge, and Y. Pan, "Rapid assessment of building damage using multi-source data: A case study of April 2015 Nepal earthquake," *Remote Sens.*, vol. 14, no. 6, pp. 398–417, Apr. 2022, doi: 10.3390/rs14061358.

[2] Y. Chen, M. Xu, X. Shen, G. Zhang, Z. Lu, and J. Xu, "A multi-objective modeling method of multi-satellite imaging task planning for large regional mapping," *Remote Sens.*, vol. 12, no. 3, p. 344, Jan. 2020, doi: 10.3390/rs12030344.

[3] J. Hu, H. Huang, L. Yang, and Y. Zhu, "A multi-objective optimization framework of constellation design for emergency observation," *Adv. Space Res.*, vol. 67, no. 1, pp. 531–545, Jan. 2021, doi: 10.1016/j.asr.2020.09.031.

[4] Y. Du, L. Xing, J. Zhang, Y. Chen, and Y. He, "MOEA based memetic algorithms for multi-objective satellite range scheduling problem," *Swarm Evol. Comput.*, vol. 50, Nov. 2019, Art. no. 100576, doi: 10.1016/j.swevo.2019.100576.

[5] G. Zhang, X. Li, G. Hu, Z. Zhang, J. An, and W. Man, "Mission planning issues of imaging satellites: Summary, discussion, and prospects," *Int. J. Aerosp. Eng.*, vol. 2021, pp. 1–20, Dec. 2021, doi: 10.1155/2021/7819105.

[6] J. Wei and L. Yan, "Research on emergency mission planning model and algorithm of networking autonomous imaging satellite," in *Proc. Int. Conf. Natural Comput., Fuzzy Syst. Knowl. Discovery*, 2021, vol. 14, no. 9, pp. 179–187, doi: 10.1007/978-3-030-70665-4_21.

[7] E. Zhibo, R. Shi, L. Gan, H. Baoyin, and J. Li, "Multi-satellites imaging scheduling using individual reconfiguration based integer coding genetic algorithm," *Acta Astronaut.*, vol. 178, no. 1, pp. 645–657, Jan. 2021, doi: 10.1016/j.actaastro.2020.08.041.

[8] X. Niu, H. Tang, and L. Wu, "Satellite scheduling of large areal tasks for rapid response to natural disaster using a multi-objective genetic algorithm," *Int. J. Disaster Risk Reduction*, vol. 28, pp. 813–825, Jun. 2018, doi: 10.1016/j.ijdrr.2018.02.013.

[9] X. Chen, G. Reinelt, G. Dai, and A. Spitz, "A mixed integer linear programming model for multi-satellite scheduling," *Eur. J. Oper. Res.*, vol. 275, no. 2, pp. 694–707, Jun. 2019, doi: 10.1016/j.ejor.2018.11.058.

[10] J. C. Pemberton and F. Galiber, "A constraint-based approach to satellite scheduling," *Eur. J. Oper. Res.*, vol. 275, no. 2, pp. 101–114, 2001, doi: 10.1090/dimacs/057/06.

[11] K. Wu, D. Zhang, Z. Chen, J. Chen, and X. Shao, "Multi-type multi-objective imaging scheduling method based on improved NSGA-III for satellite formation system," *Adv. Space Res.*, vol. 63, no. 8, pp. 2551–2565, Apr. 2019, doi: 10.1016/j.asr.2019.01.006.

[12] H. Chen, B. Zhai, J. Wu, C. Du, and J. Li, "A satellite observation data transmission scheduling algorithm oriented to data topics," *Int. J. Aerosp. Eng.*, vol. 2020, no. 8, pp. 1–16, Jul. 2020, doi: 10.1155/2020/2180674.

[13] J. Zhang, L. Xing, G. Peng, F. Yao, and C. Chen, "A large-scale multiobjective satellite data transmission scheduling algorithm based on SVM+NSGA-II," *Swarm Evol. Comput.*, vol. 50, Nov. 2019, Art. no. 100560, doi: 10.1016/j.swevo.2019.100560.

[14] B. Du and S. Li, "A new multi-satellite autonomous mission allocation and planning method," *Acta Astronaut.*, vol. 163, pp. 287–298, Oct. 2019, doi: 10.1016/j.actaastro.2018.11.001.

[15] J. Wang, E. Demeulemeester, and D. Qiu, "A pure proactive scheduling algorithm for multiple Earth observation satellites under uncertainties of clouds," *Comput. Oper. Res.*, vol. 74, pp. 1–13, Oct. 2016, doi: 10.1016/j.cor.2016.04.014.
[16] Y. She, S. Li, and Y. Zhao, "Onboard mission planning for agile satellite using modified mixed-integer linear programming," *Aerosp. Sci. Technol.*, vol. 72, pp. 204–216, Jan. 2018, doi: 10.1016/j.ast.2017.11.009.
[17] J. Liang, Y.-H. Zhu, Y.-Z. Luo, J.-C. Zhang, and H. Zhu, "A precedence-rule-based heuristic for satellite onboard activity planning," *Acta Astronaut.*, vol. 178, pp. 757–772, Jan. 2021, doi: 10.1016/j.actaastro.2020.10.020.
[18] Y. Chen, J. Lu, R. He, and J. Ou, "An efficient local search heuristic for Earth observation satellite integrated scheduling," *Appl. Sci.*, vol. 10, no. 16, p. 5616, Aug. 2020, doi: 10.3390/app10165616.
[19] Y. He, Y. Chen, J. Lu, C. Chen, and G. Wu, "Scheduling multiple agile Earth observation satellites with an edge computing framework and a constructive heuristic algorithm," *J. Syst. Archit.*, vol. 95, pp. 55–66, May 2019, doi: 10.1016/j.sysarc.2019.03.005.
[20] Y.-J. Song, X. Ma, X.-J. Li, L.-N. Xing, and P. Wang, "Learning-guided nondominated sorting genetic algorithm II for multi-objective satellite range scheduling problem," *Swarm Evol. Comput.*, vol. 49, pp. 194–205, Sep. 2019, doi: 10.1016/j.swevo.2019.06.008.
[21] G. Wu, R. Mallipeddi, and P. N. Suganthan, "Ensemble strategies for population-based optimization algorithms—A survey," *Swarm Evol. Comput.*, vol. 44, pp. 695–711, Feb. 2019, doi: 10.1016/j.swevo.2018.08.015.
[22] Z. Zheng, J. Guo, and E. Gill, "Swarm satellite mission scheduling & planning using hybrid dynamic mutation genetic algorithm," *Acta Astronaut.*, vol. 137, pp. 243–253, Aug. 2017, doi: 10.1016/j.actaastro.2017.04.027.
[23] Q. Luo, W. Peng, G. Wu, and Y. Xiao, "Orbital maneuver optimization of Earth observation satellites using an adaptive differential evolution algorithm," *Remote Sens.*, vol. 14, no. 9, p. 1966, Apr. 2022, doi: 10.3390/rs14091966.
[24] H. Sun, W. Xia, Z. Wang, and X. Hu, "Agile Earth observation satellite scheduling algorithm for emergency tasks based on multiple strategies," *J. Syst. Sci. Syst. Eng.*, vol. 30, no. 5, pp. 626–646, Oct. 2021, doi: 10.1007/s11518-021-5506-4.
[25] M. Chen, J. Wen, Y.-J. Song, L.-N. Xing, and Y.-W. Chen, "A population perturbation and elimination strategy based genetic algorithm for multi-satellite TT&C scheduling problem," *Swarm Evol. Comput.*, vol. 65, Aug. 2021, Art. no. 100912, doi: 10.1016/j.swevo.2021.100912.
[26] Z. Li, L. Zhao, Y. Liu, X. Chen, H. Chen, F. Zheng, Y. Zhang, D. Wang, J. Li, J. Liu, and S. Liu, "Autonomous mission planning method for optical imaging satellites based on real-time cloud cover information," *Remote Sens.*, vol. 14, no. 11, p. 2635, May 2022, doi: 10.3390/rs14112635.
[27] Y. Yu, Q. Hou, J. Zhang, and W. Zhang, "Mission scheduling optimization of multi-optical satellites for multi-aerial targets staring surveillance," *J. Franklin Inst.*, vol. 357, no. 13, pp. 8657–8677, Sep. 2020, doi: 10.1016/j.jfranklin.2020.06.023.
[28] Z. Zeng, M. Zhang, T. Chen, and Z. Hong, "A new selection operator for differential evolution algorithm," *Knowl.-Based Syst.*, vol. 226, Aug. 2021, Art. no. 107150, doi: 10.1016/j.knosys.2021.107150.
[29] R. D. Al-Dabbagh, F. Neri, N. Idris, and M. S. Baba, "Algorithmic design issues in adaptive differential evolution schemes: Review and taxonomy," *Swarm Evol. Comput.*, vol. 43, pp. 284–311, Dec. 2018, doi: 10.1016/j.swevo.2018.03.008.
[30] M. Wang, Y. Ma, and P. Wang, "Parameter and strategy adaptive differential evolution algorithm based on accompanying evolution," *Inf. Sci.*, vol. 607, pp. 1136–1157, Aug. 2022, doi: 10.1016/j.ins.2022.06.040.
[31] G. Sun, B. Yang, Z. Yang, and G. Xu, "An adaptive differential evolution with combined strategy for global numerical optimization," *Soft Comput.*, vol. 24, no. 9, pp. 6277–6296, May 2020, doi: 10.1007/s00500-019-03934-3.
[32] X. Xia, L. Gui, Y. Zhang, X. Xu, F. Yu, H. Wu, B. Wei, G. He, Y. Li, and K. Li, "A fitness-based adaptive differential evolution algorithm," *Inf. Sci.*, vol. 549, pp. 116–141, Mar. 2021, doi: 10.1016/j.ins.2020.11.015.
[33] J. Cui and X. Zhang, "Application of a multi-satellite dynamic mission scheduling model based on mission priority in emergency response," *Sensors*, vol. 19, no. 6, p. 1430, Mar. 2019, doi: 10.3390/s19061430.

XUEYING YANG was born in 1998. She received the B.S. degrees from Nanchang Hangkong University, Nanchang, China, in 2016 and 2020, and the M.S. degrees from the Belarusian State University of Informatics and Radio-Electronics, Belarus, in 2020 and 2022. She is currently pursuing the Ph.D. degree with Space Engineering University, Beijing, China. Her research interests include multi-satellite mission planning and scheduling.

MIN HU was born in 1983. He received the B.S. and M.S. degrees from the Equipment College, China, in 2006 and 2008, respectively, and the Ph.D. degree from Space Engineering University, Beijing, China, in 2012. He is currently an Associate Professor with Space Engineering University. He has published more than 60 articles and authorized 25 national invention patents. His research interests include spacecraft orbit dynamics, distributed spacecraft dynamics and control, the design of constellation, and space mission analysis.

RUI ZHANG was born in Sichuan, China, in 1989. He received the B.S. degree in automation from the University of Electronic Science and Technology of China, Chengdu, China, in 2012, and the M.S. and Ph.D. degrees in aerospace science and technology from the National University of Defense Technology, Changsha, China, in 2014 and 2019, respectively. From 2015 to 2019, he studied with Tsinghua University as a Joint Training Student. Since December 2019, he has been a Lecturer with Space Engineering University, Beijing, China. He has published 11 papers and authorized three patents. His research interests include distributed space systems and artificial intelligence.

GANG HUANG was born in Jiangsu, China, in 1991. He received the bachelor's degree from the Jincheng College, Nanjing University of Aeronautics and Astronautics, in 2015, and the master's degree from Nanchang Hangkong University, in 2020. He is currently pursuing the Ph.D. degree with Space Engineering University. His research interests include evolutionary computing and intelligent collaboration.